Journal of Catalysis 257 (2008) 64–70

Contents lists available at ScienceDirect

Journal of Catalysis

www.elsevier.com/locate/jcat

Stability of bimetallic Pd–Zn catalysts for the steam reforming of methanol

Travis Conant [a], Ayman M. Karim [a], Vanessa Lebarbier [a,b], Yong Wang [b], Frank Girgsdies [c], Robert Schlögl [c], Abhaya Datye [a,*]

[a] Department of Chemical and Nuclear Engineering, Center for Micro Engineered Materials, University of New Mexico, Albuquerque, NM, USA
[b] Pacific Northwest National Lab Richland, WA, USA
[c] Fritz-Haber-Institut der Max-Planck-Gesellschaft Faradayweg 4-6, Berlin, Germany

ARTICLE INFO

Article history:
Received 21 December 2007
Revised 9 April 2008
Accepted 11 April 2008
Available online 2 June 2008

Keywords:
Methanol steam reforming
PdZn alloy
STEM
EDS
FTIR
XRD

ABSTRACT

ZnO-supported palladium-based catalysts have been shown in recent years to be both active and selective towards the steam reforming of methanol, although they are still considered to be less active than traditional copper-based catalysts. The activity of PdZn catalysts can be significantly improved by supporting them on alumina. Here we show that the $Pd/ZnO/Al_2O_3$ catalysts have better long-term stability when compared with commercial $Cu/ZnO/Al_2O_3$ catalysts, and that they are also stable under redox cycling. The $Pd/ZnO/Al_2O_3$ catalysts can be easily regenerated by oxidation in air at 420 °C followed by re-exposure to reaction conditions at 250 °C, while the Cu/ZnO based catalysts do not recover their activity after oxidation. Reduction at high temperatures (>420 °C) leads to Zn loss from the alloy nanoparticle surface resulting in a reduced catalyst activity. However, even after such extreme treatment, the catalyst activity is regained with time on stream under reaction conditions alone, leading to highly stable catalysts. These findings illustrate that the nanoparticle surface is dynamic and changes drastically depending on the environment, and that elevated reduction temperatures are not necessary to achieve high CO_2 selectivity.

1. Introduction

As electronic devices become smaller and more complex, hydrogen-fed compact fuel cell systems become a feasible solution for the resulting power requirements, replacing current Li-ion batteries. The on-board storage of pressurized hydrogen is inherently problematic for a mobile device because of an increased balance-of-plant resulting in a lowered overall power density of the device. Methanol is considered an ideal choice for on-demand production of hydrogen because it is sulfur-free and can be reformed at lower temperatures (200–250 °C) than most other fuels since it contains no carbon–carbon bonds that must be broken [1]. Although most early studies on the steam reforming of methanol were focused on copper-based catalysts since they are the industrial standard for methanol synthesis [2], the current focus has shifted away from copper due to its fast deactivation (Fig. 1), poor thermal stability, and pyrophoric nature.

While Cu is known to be highly active and selective towards the steam reforming of methanol, group VIII metals, such as Pd, favor methanol decomposition to CO and H_2 [3]. Iwasa et al. were the first to report that Pd became highly active for reforming and selective towards CO_2 when supported on ZnO and reduced at temperatures above 300 °C [4–10]. This was attributed to the bulk PdZn alloy which was formed by the spill-over of atomic hydrogen from the Pd metal to the ZnO, leading to facile reduction of the ZnO and migration of Zn to the metallic surface [5,9]. A number of studies [11–15] have investigated how the electronic structure changes from Pd to PdZn alloys, along with the similarities between Cu and PdZn from an electronic structure standpoint. Previous work has shown that the extent of alloy formation increased with higher reduction temperatures [5,16]. However, our recent research has shown that the selectivity towards CO_2 does not monotonically increase with the extent of alloy formation [16]. An understanding of the effect of surface characteristics on catalyst performance would provide further insight into what is occurring at the nanoscale during the steam reforming of methanol.

In this work, we prepared $Pd/ZnO/Al_2O_3$ catalysts which were exposed to a number of pretreatments. The catalysts were supported on alumina in order to stabilize the particles against sintering at elevated temperatures, as is seen with Pd/ZnO catalysts [16], and to avoid the effects of particle size changes on catalyst activity. Our goal was to understand the variation between bulk and surface compositions of PdZn catalysts and the resulting relationship to catalyst performance, deactivation, and regeneration. The crystallite size and composition were studied using scanning transmission electron microscopy (STEM) and energy dispersive X-ray spectroscopy (EDS). The bulk composition was determined by X-ray diffraction (XRD), while the average surface composition was analyzed by using Fourier transform infrared spectroscopy (FTIR). As

* Corresponding author. Fax: +1 505 277 0477.
E-mail address: datye@unm.edu (A. Datye).

0021-9517/$ – see front matter
doi:10.1016/j.jcat.2008.04.018

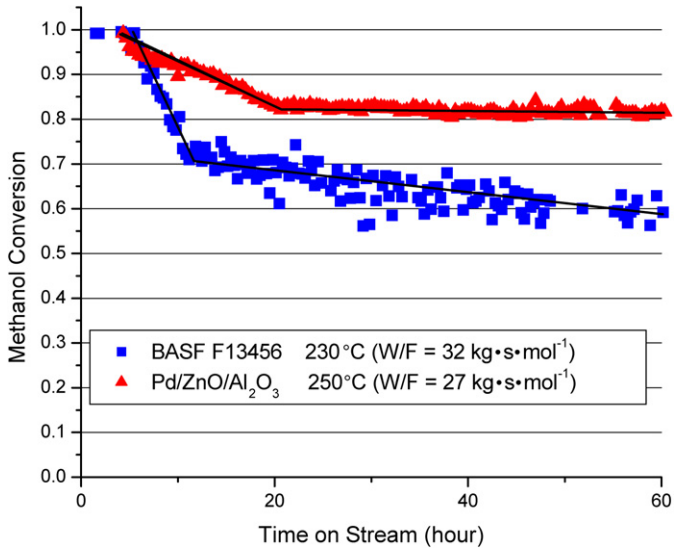

Fig. 1. Activity over 60 h comparison between commercial Cu-based catalyst (BASF F13456) and $Pd/ZnO/Al_2O_3$. The Cu-based catalyst suffers from fast deactivation, whereas the Pd-based catalyst deactivates to a lesser extent. However, the activity of the Pd-based catalyst is initially lower and it is tested at 250 °C where the Cu-based catalyst is active at 230 °C.

we show in this work, the composition uniformity within individual particles is improved with increasing reduction temperatures up to 300 °C, while higher reduction temperatures (>500 °C) lead to Zn depletion from the surface resulting in lowered performance. However, the Zn-depleted catalyst surface can be regenerated simply by exposure to reaction conditions. Furthermore, deactivated catalysts can be regenerated by a short oxygen treatment followed by exposure to reaction conditions. These results suggest that the catalyst surface is dynamic, and that pretreatments result in a meta-stable state which reaches equilibrium under reaction conditions giving this catalyst system its remarkable stability.

2. Experimental

2.1. Catalyst preparation

We prepared $Pd/ZnO/Al_2O_3$ catalysts by an incipient wetness technique. The Al_2O_3 was first prepared by calcining boehmite (Sasol) at 850 °C for 5 h. A solution of Pd and Zn nitrates (Pd/Zn molar ratio = 0.38) was added drop wise to the Al_2O_3 and the mixture was shaken to ensure even distribution of the nitrate precursor. This was followed by drying at 80 °C, and the process was repeated until 8.8 wt% Pd was achieved. The dried catalyst is designated "as-prepared."

2.2. Reactivity measurements

Measurements of the steam-reforming of methanol were performed in a tubular packed-bed reactor. The catalyst was crushed and sieved to 100–250 μm and packed into a reactor consisting of a quartz tube of inner diameter (i.d.) 1.75 mm. The reactor was positioned in an insulated programmable oven. The temperature of the reactor outer surface was measured as well as the reactor inlet and outlet temperatures. The reactor effluent stream passed through a gas-sampling valve, then through a condenser to trap unreacted water and methanol before reaching a digital mass flow meter which allowed for total dry product gas flow to be monitored. The effluent of the reactor was analyzed using a Varian CP-3800 gas chromatograph (GC) equipped with a Porapak Q column and a TCD detector, using helium as the carrier gas. The analysis of the gas phase species CO_2, CO and CH_3OH along with a carbon balance allowed the methanol conversion and CO_2 selectivity to be calculated. The GC was programmed to sample reactor product gases at 20 min intervals. The entire system was automated by Labview software and appropriate data acquisition hardware.

The material balance was done as follows: Using the methanol conversion and CO_2 selectivity and the reaction network stoichiometry, the total theoretical dry gas flow rate was calculated and compared to the reading of the mass flow meter. The agreement was very good, indicating that no carbon is deposited on the catalyst. Prior to the reaction, the catalyst was pretreated under different conditions as explained in the results section. After pretreatment, the catalyst was brought to the reaction temperature of 250 °C under helium flow. A mixture of 1.1:1 molar water/methanol was then pumped using a syringe pump (Cole Parmer 74900) at 0.2 mL/h to an in-house built vaporizer operating at 130 °C. The vaporizer was optimized to get a stable flow rate and minimize fluctuations in the water–methanol molar ratio. After starting the methanol/water liquid flow, 15 to 30 min were allowed for the flow rate to stabilize before injecting samples into the GC. The product distribution was monitored while changing the flow rate of the liquid water/methanol mixture from low to high flow rate.

2.3. Catalyst characterization

Scanning and high-resolution transmission electron microscopy (STEM and HRTEM) were performed on a JEOL 2010F FASTEM field emission gun scanning transmission electron microscope. Compositional variance was determined by energy dispersive X-ray spectroscopy (EDS) in the STEM mode. The probe size was 1.0 nm, allowing us to scan the composition within individual metal crystallites. The samples were analyzed also by in situ X-ray diffraction (XRD) to determine bulk compositions of Pd and PdZn using under various atmospheres using a Bruker AXS D8 Advance diffractometer (θ/θ geometry, secondary graphite monochromator, scintillation counter) using Cu$K\alpha$ radiation. The setup was equipped with an Anton Paar HTK 16 high temperature chamber in which the sample was dispersed on a resistance heated Inconel band. A controlled gas atmosphere with a total flow of 100 ml/min was achieved using Bronkhorst mass flow controllers and the effluent gas was monitored by means of a quadrupole mass spectrometer (Pfeiffer OmniStar). A typical scan was done over a range from 30°–50° 2θ, with a 0.03° step size, and a 5 s dwell time. The surface composition of the catalysts (amount of metallic Pd and PdZn alloy) was examined by CO adsorption at room temperature followed by Fourier transform infrared (FTIR) spectroscopy. The samples were pressed into a pellet for analysis and IR spectra were recorded using a Nicolet Magna 750 spectrometer equipped with a Mercury Cadmium Telluride detector (resolution; 4 cm^{-1}, 128 scans).

3. Results

3.1. Catalyst deactivation and regeneration

All data reported in this section refer to catalysts exposed to a 1.1:1 mixture of water and methanol at a flow rate of 0.2 mL/h. Approximately 30 mg of the $Pd/ZnO/Al_2O_3$ catalyst (corresponding to W/F of 32 kg s mol^{-1}) and 25 mg of BASF F13456 Cu/ZnO-based catalyst (corresponding to W/F of 27 kg s mol^{-1}) were tested in these experiments. It is important to note that the Pd/Zn-based catalyst was tested at 250 °C whereas the Cu/ZnO-based catalyst was tested at 230 °C. Fig. 1 shows the activity over 60 h for both the commercial $Cu/ZnO/Al_2O_3$ catalyst (BASF F13456) and our $Pd/ZnO/Al_2O_3$. The Cu/ZnO-based catalyst suffers from fast initial deactivation, followed by a continual long-term deactivation. Overall, there is a 40% drop in the conversion of the Cu/ZnO-based

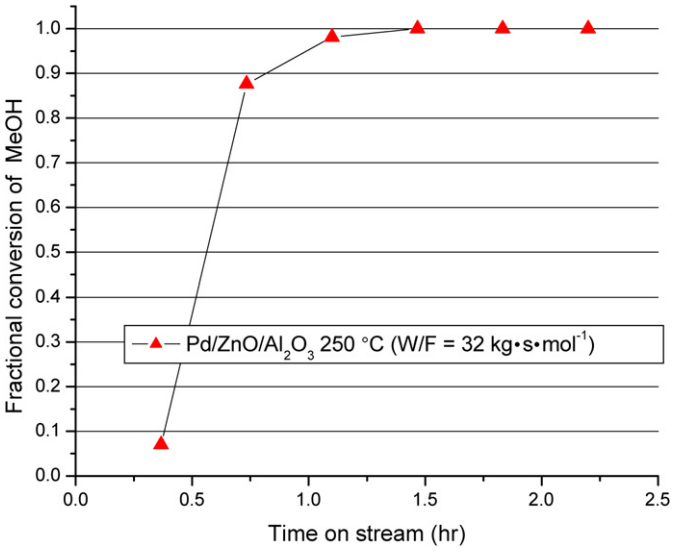

Fig. 2. Regeneration of a deactivated $Pd/ZnO/Al_2O_3$ catalyst after oxidation at 420 °C and exposure to steam reforming conditions at 250 °C. The catalyst is found to regain its initial activity within approximately 1 h on stream.

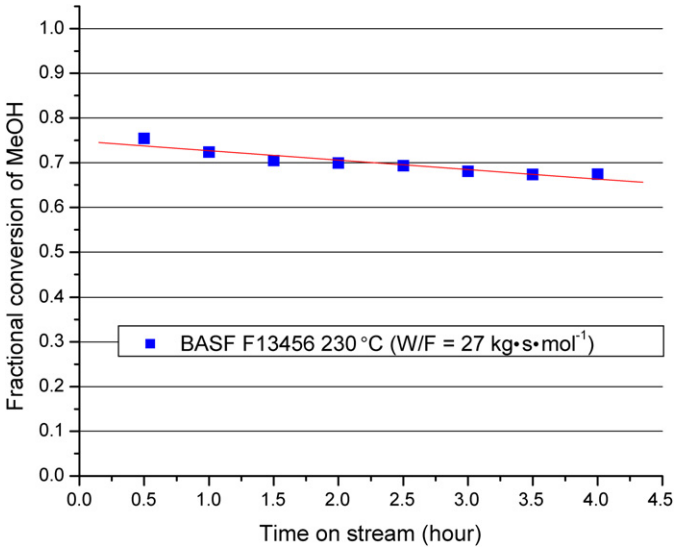

Fig. 3. The deactivated Cu-based commercial catalysts (BASF F13456) did not regain its initial activity after oxidation in air at 420 °C followed by exposure to steam reforming conditions.

catalyst after 60 h time on stream. The drop in the activity of the Pd/ZnO-based catalyst is not attributed to sintering as the average diameter only increases to approximately 4.9 nm. Furthermore, it has been previously reported that an increase in PdZn alloy crystallite size with increasing reduction temperature had no adverse impact on catalytic behavior of Pd/ZnO catalysts [16].

On the other hand, the Pd/ZnO-based catalyst seemingly only suffers from the initial deactivation period (where there is only a 17% drop in conversion), and is stable after this initial drop out to 60 h of time on stream. For the palladium-based catalyst we found that a simple oxidation–reduction cycle could regenerate the catalyst and that the initial activity was fully recovered. The deactivated catalyst was oxidized in air at 420 °C for 4 h and then exposed directly to steam reforming conditions. It can be seen in Fig. 2 that the catalyst regains its original activity within the first hour on stream. The first data point on this figure can be ascribed to the initial reduction of the PdO to Pd. It has been shown that methanol steam reforming over Pd has a much lower reaction rate [16] which explains the initial 8% conversion. This was also confirmed by the selectivity of the re-reduced catalyst. The selectivity to CO_2 was found to be only 67% when the conversion was at 8%, and then quickly increased to 95% where it remained stable with time on stream. When the copper/ZnO-based catalyst underwent the same oxidation treatment, the catalyst was not regenerated and it continued to lose activity with time on stream, Fig. 3. Moreover, it was found that the CO_2 selectivity for the Cu/ZnO-based catalyst remained constant at approximately 96% regardless of the treatments, which is indicative of metallic Cu being the active site.

3.2. In situ XRD

The as-prepared catalyst was ramped (at 10 °C/min) to a given reduction temperature, and was held at each temperature for 2 h while concurrently taking two XRD scans. Fig. 4 summarizes the XRD data for the in situ reduction scans. The (111) peaks for Pd and PdZn are identified on the graph at 2θ values of 40.16° and 41.23°, respectively, along with the (110) peak of $Pd_{1.35}Zn_{0.65}$ at 41.78° (ICDD card #46-1043 for Pd, #06-0620 for PdZn, and ICSD card #105754 for $Pd_{1.35}Zn_{0.65}$). Our previous report [16] showed that when supported on ZnO, the PdZn alloy did in fact have the stoichiometry of 1:1, yet we show here that when supported on Al_2O_3 only the first reflection can be identified via XRD due to the high background associated with the Al_2O_3 support. Due to the broadness of the peak and the background in the XRD patterns, the PdZn and $Pd_{1.35}Zn_{0.65}$ phases are very difficult to identify conclusively via XRD. Therefore, we will call this a Pd–Zn alloy throughout the rest of this manuscript. After reduction at 150 °C, the catalyst is seen to be predominantly bulk Pd, although the right shoulder on the peak is most likely attributed to small amounts of Pd–Zn. As the reduction temperature is increased, there is a shift towards the Pd–Zn with a complete shift at temperatures above 330 °C. At higher temperatures (up to 500 °C), there appears to be a further sharpening of the Pd–Zn peak which is attributed to both an increase in crystallite size and better ordering of the Pd–Zn alloy (both of which will be discussed in the following section).

3.3. TEM, STEM, and EDS

We used high angle annular dark field imaging (HAADF) in the STEM mode to detect and analyze particle sizes in the Pd-based catalysts. From STEM images, we counted a few hundred particles to determine the number-average particle size and standard deviation of the mean for each sample, Fig. 5. The 1.0 nm probe in our STEM was used to determine compositions from the near-surface region as well as the center of each particle. EDS analysis becomes crucial in relating reactivity data to particle size and nanoparticle compositional uniformity. However, when analyzing such small volumes, we get few counts, making it difficult to derive accurate elemental compositions. Therefore we have reported our data in terms of the Pd/Zn ratios obtained from the center and the edge of approximately 15–20 particles in each sample. In order to normalize the ratio from center to edge in each particle, we have used the following formula:

$$\frac{\text{center}}{\text{edge}} = \left(\frac{Pd_{\text{center}}/Zn_{\text{center}}}{Pd_{\text{edge}}/Zn_{\text{edge}}} \right)$$

When this ratio is greater than 1, the particle is Zn-rich at the surface; when it equals 1, the particle has a uniform composition throughout; and when it is less than 1, the particle is Zn-deficient at the surface.

Table 1 summarizes both the STEM and EDS data. The average particle size derived from STEM analysis increases from 2.5 nm

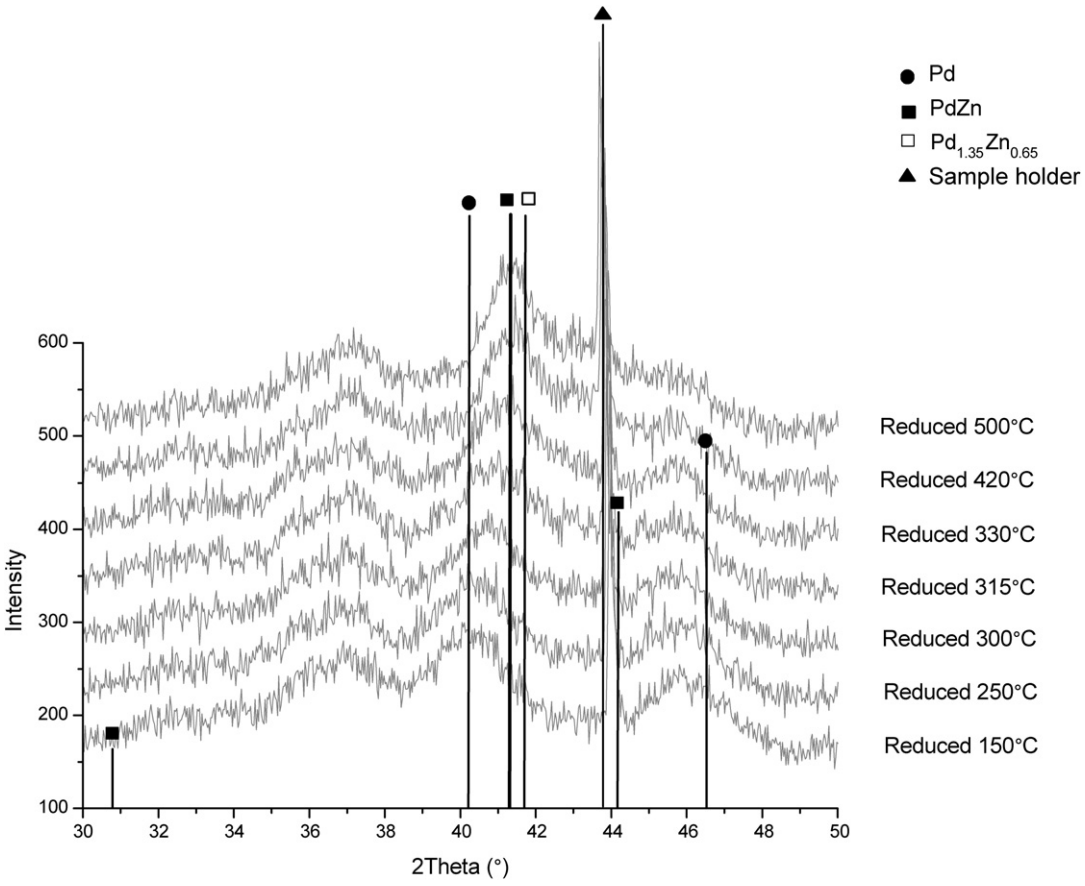

Fig. 4. XRD patterns of $Pd/ZnO/Al_2O_3$ catalysts reduced in situ at various temperatures. The relative amounts of bulk Pd and Pd–Zn change as the catalyst is reduced at elevated temperature. Note that the sharp peak at 44° 2θ is attributed to the metallic sample holder.

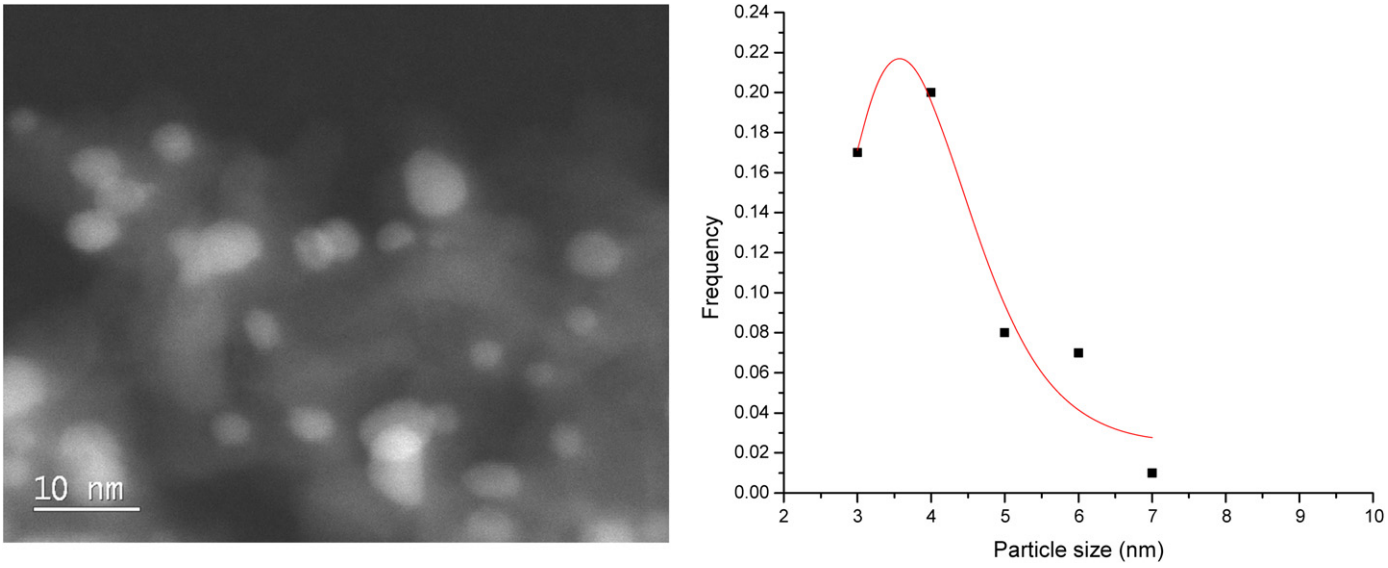

Fig. 5. HAADF STEM image of 8.8 wt% $Pd/ZnO/Al_2O_3$ reduced at 420 °C for 2 h. The particle size distribution of this catalyst is shown; the number average diameter is 3.6 nm.

when reduced at 150 °C up to 4.7 nm when reduced at 500 °C. This increase is due in part to catalyst sintering, but also due to the increased volume of each particle as Zn is incorporated into the lattice structure. Overall EDS analysis of particles revealed that the Pd:Zn ratio is approximately 2:1 when supported on Al_2O_3 where it has been previously shown that this ratio is 1:1 when supported on ZnO [5,16]. The EDS data also show that the alloy forms first at the surface and then propagates inward. This is similar to the Pd–Zn alloy formation described on model catalysts in the literature [17], and is in agreement with density functional theory modeling done for Pd–Zn systems prepared by placing a monolayer of Pd on a ZnO (0001) substrate [18]. When the catalyst was reduced at 150 °C, the Zn counts were extremely low and the data is therefore unreliable, so it has been omitted in this analysis. For the catalyst reduced at 250 °C, the average center/edge ratio was found to be over two meaning that the catalyst surface was

Table 1
Summary of STEM and EDS data for $Pd/ZnO/Al_2O_3$ catalysts exposed to various reduction temperatures

H_2 reduction	150 °C	250 °C	300 °C	315 °C	330 °C	420 °C	500 °C
Number average particle diameter (nm) (STEM)	2.5	2.3	2.8	2.9	3.3	3.7	4.7
Standard deviation of the number average particle size (nm)	0.7	0.5	0.7	0.9	1.1	1.1	1.4
Average center/edge ratio of Pd/Zn	[a]	2.5 ± 1.7	1.1 ± 0.4	1.0 ± 0.3	1.0 ± 0.4	0.7 ± 0.1	0.7 ± 0.2

[a] Too few Zn counts.

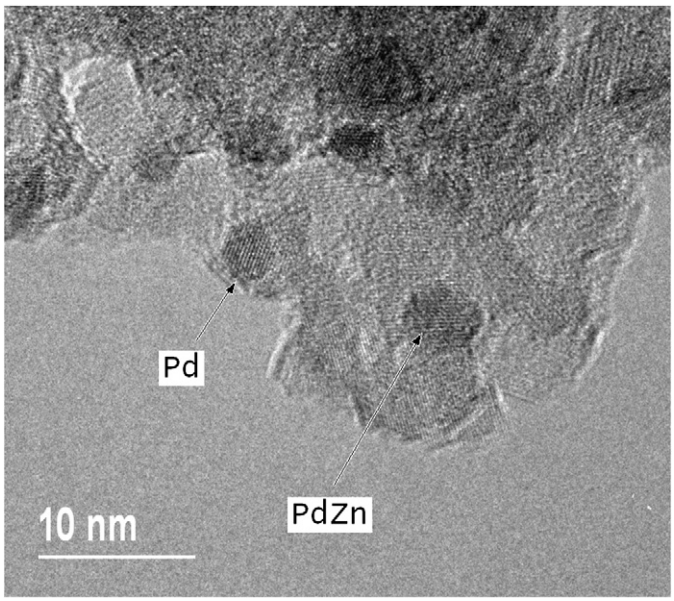

Fig. 6. HRTEM image of $Pd/ZnO/Al_2O_3$ catalysts reduced at 250 °C. This image illustrates that both bulk PdZn and Pd nanoparticles can be identified within close proximity via cross-fringe analyses. It is also evident that the nanoparticles are not seen to be core-and-shell, although the EDX data shows a large variation between the near-edge and bulk compositions when reduced at this temperature.

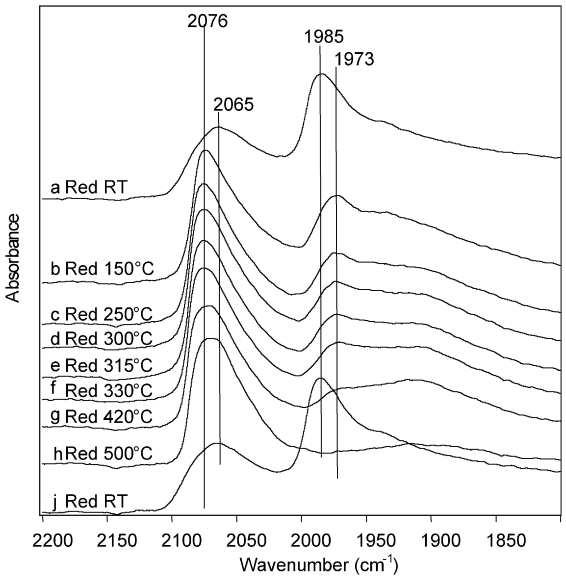

Fig. 7. IR spectra for $Pd/ZnO/Al_2O_3$ catalysts undergoing an oxidation–reduction cycle. Note that between scans (h) and (j) the sample was oxidized at 500 °C for 2 h, followed by reduction at room temperature for 2 h in H_2. The peaks associated with Pd–CO (linear: 2065 cm^{-1}, bridged: 1985 cm^{-1}) and Pd–Zn (linear: 2076 cm^{-1}) can be clearly identified in these spectra. The formation of the Pd–Zn occurs readily even at low temperatures. Oxidation recreates the Pd surface.

Zn-rich, when compared to the bulk. Fig. 6 shows a high resolution transmission electron microscopy image which illustrates the nanostructure of the particles after reduction at 250 °C. It can be seen that there is no core-and-shell structure formed although the EDS data show a variance between the near-surface and bulk compositions.

As the reduction temperature increases to 330 °C, this ratio drops to 1, which illustrates the propagation of the Zn inwards from the outer surface, resulting in a more uniform composition. The compositional variation from particle to particle also decreased with increased reduction temperature, which is evident by the drop in the standard deviation of the center/edge ratio as reduction temperature is increased. However, as the temperature is increased to 420 °C and further to 500 °C, the center/edge ratio drops below 1 due to depletion of Zn from the surface. J.A. Rodriguez [14] reported on the thermal stability of thick Pd–Zn alloys deposited on a Ru (001) substrate using thermal decomposition mass spectroscopy. This author found that the decomposition mechanism released Zn into the gas phase at temperatures varying from 147 to 727 °C. It was found that Zn-rich alloys were less stable with decomposition at lower temperatures, while Pd-rich alloys were stable up to 727 °C. Again, our 2:1 Pd–Zn alloys were found to be stable up to approximately 420 °C. This difference between the reported data [14] and ours can be explained by the Gibbs–Thompson relation where the volatility of materials increases with decrease in particle size. With such changes in the near-surface composition elucidated by EDS analysis, FTIR of adsorbed CO is crucial in probing the actual surface composition.

3.4. FTIR of absorbed CO

The as-prepared catalyst was first reduced at 500 °C and then calcined in air to remove the nitrate precursors. The calcined catalyst was exposed to an oxidation–reduction cycle at temperatures ranging from room temperature to 500 °C while intermittently obtaining IR scans at each temperature. Note that after the initial reduction up to 500 °C, the catalyst was again oxidized and re-reduced at room temperature. The results of the oxidation–reduction cycle are summarized in Fig. 7. When the calcined sample is initially reduced at room temperature, bands corresponding to CO absorbed on metallic Pd were observed at 1985 and 2065 cm^{-1}, which are assigned to bridge and linear-bound CO, respectively [19–22]. However, as the reduction temperature is raised, we see the loss of bridge-bonded CO peaks due to ensemble effects as neighboring Pd atoms are lost when Zn is incorporated. There is also a measurable shift in the linear-bound CO frequency from 2065 cm^{-1} for Pd to 2076 cm^{-1} for Pd–Zn due to ligand effects. The assignment of the CO band on Pd–Zn is based on recent literature assignments derived from single crystal surfaces as well as high surface area catalysts [23,24]. The ligand effects were reported by Tsai et al. [15] due to the differences in the density of states between Pd and Pd–Zn as calculated from density functional theory. The peak associated with linear-bound CO on Pd–Zn

remains sharp at reduction temperatures up to 330 °C, yet as the temperature is raised up to 420 °C, the peak begins to broaden and encompass the frequency associated with linear-bound CO on metallic Pd as well. This trend continues as the reduction temperature is increased further to 500 °C, again suggesting loss of Zn from the surface at elevated reduction temperatures. When the reduced sample is oxidized at 500 °C for 2 h and then reduced again at room temperature, the sample shows CO peaks indicative of monometallic Pd. The oxidation process therefore serves to break apart the alloy into PdO and ZnO, which upon reduction in H_2 reforms readily to Pd metal.

3.5. Steam reforming of methanol

Table 2 summarizes the steam reforming reactivity for two different catalysts; one underwent reduction at 400 °C for 2 h, while the other was the as-prepared sample. The data is reported at an identical W/F of 18.44 kg s mol^{-1} in order to properly compare the reactivity of these two catalysts. CO_2 selectivity is defined as moles of CO_2 in the effluent divided by the number of moles of $CO + CO_2$. It can be seen that these two catalysts exhibit similar activity and selectivity even though these different pretreatments undoubtedly result in different bulk compositions. The turn-over frequency (TOF) for the bimetallic catalysts was estimated from the dispersion calculated from the average crystallite diameter and assuming that the nanoparticle was composed of a uniform 2:1 Pd–Zn alloy. The TOF was estimated to be 0.39 s^{-1}, which is comparable to the value of 0.8 s^{-1} reported in the literature for Pd/ZnO catalysts [25]. As a comparison, the TOF for $Cu/ZnO/Al_2O_3$ catalysts reported in the literature has been reported to range from 0.0152 [26] to 0.11 s^{-1} [27]. After 4 h of exposure to steam reforming conditions, both these catalysts were analyzed via FTIR of adsorbed CO. Fig. 8 shows that the surfaces of the two catalysts give nearly identical IR spectra after reaction. Note that the major peak for both catalysts comes from atop CO at ~2070 cm^{-1} (and a very small peak corresponding to the bridge-bonded CO) confirming that the catalyst surface contains predominantly Pd–Zn in both cases [23,24]. The fact that the as-prepared catalyst shows a similar surface composition to the one reduced at 400 °C is intriguing since the as-prepared catalyst contains no Pd–Zn alloy before reaction. It can be concluded that the as-prepared catalyst must have formed a surface alloy after exposure to reaction conditions at 250 °C. Surprisingly, the final surface composition was nearly identical to the catalyst reduced at 400 °C. These results suggest that both catalysts, when exposed to reaction conditions, reach an equilibrium state which is different from that of the surface state post-reduction. This is illustrated by the fact that the IR footprints in Fig. 8 do not clearly match the IR footprints reported in Fig. 7 for the reduction cycles.

To further test this hypothesis of surface rearrangement under reaction condition exposure, we took the catalyst reduced at 500 °C, which we showed earlier to have lost Zn from the alloy surface, and tested its activity again for the steam reforming of methanol. Fig. 9 shows that the activity continually increased with time on stream, and was restored to its activity before the 500 °C reduction, again demonstrating the self-healing nature of the $Pd/ZnO/Al_2O_3$ catalysts. The CO_2 selectivity was also found to

Table 2
Reactivity comparison of two catalysts exposed to different pretreatments prior to steam reforming conditions

Reduction temp (°C)	W/F (kg s mol^{-1})	MeOH conversion (%)	CO_2 selectivity (%)
As-prepared	18.44	92.6	97.4
400	18.44	94.7	97.1

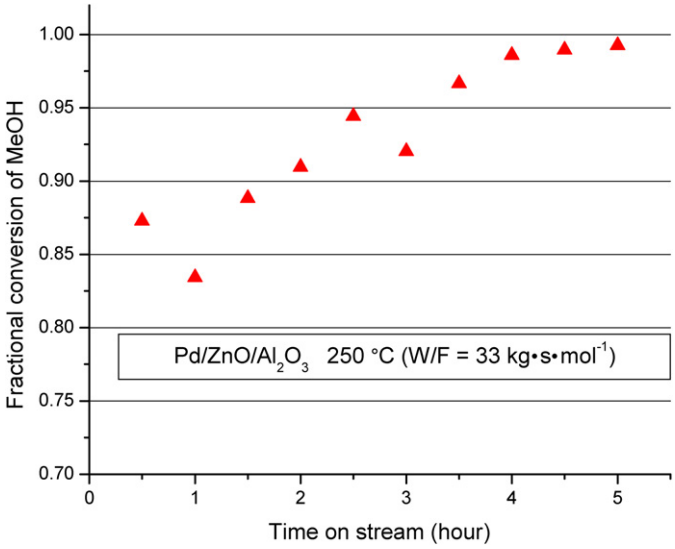

Fig. 9. Activity of the catalyst reduced at 500 °C. Although the initial conversion was quite low, the conversion increased over time until the catalyst regained its original activity after approximately 3 h. EDS shows that Zn is found to be depleted from the near-surface region at reduction temperatures above 330 °C, which causes the low activity. But the Zn within the bulk may diffuse to the surface over time, allowing the catalyst surface to reach its equilibrium state under reaction conditions, providing evidence of a self-healing catalyst.

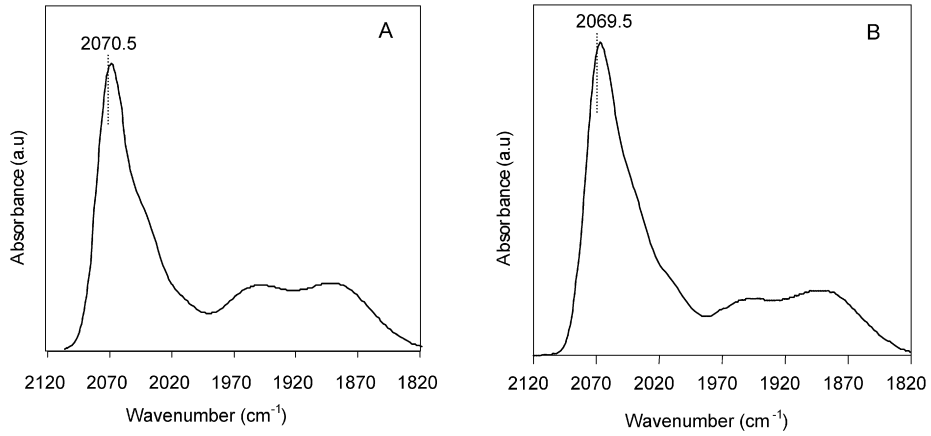

Fig. 8. IR spectra of absorbed CO for catalyst samples A and B. Catalyst A was reduced at 450 °C for 2 h before being tested for SRM at 250 °C, whereas catalyst B underwent no pretreatment. The two spectra are nearly identical and show the bands characteristic of linearly bound CO on Pd–Zn alloy, while the bands attributed to linearly bound CO on Pd are not detected. The relative ratio of the bridged to linear CO is another indication that the surface consists of the Pd–Zn alloy phase.

Table 3
EDS summary for 8.8 wt% $Pd/ZnO/Al_2O_3$ catalyst reduced at 500 °C for 2 h, pre- and post-reaction at 250 °C

H_2 reduction	500 °C (pre-reaction)	500 °C (post-reaction)
Average center/edge ratio of Pd/Zn	0.7 ± 0.2	1.0 ± 0.3

remain constant with time on stream at approximately 96%. While Zn is depleted from the surface of the nanoparticles due to the increased volatility of Zn at elevated temperatures, the nanoparticle surface manages to reach equilibrium when exposed to reaction conditions at 250 °C. In other words, the nanoparticle reorders and reforms the surface Pd–Zn alloy due to the presence of Zn within the bulk of the nanoparticle. This again is evident by the STEM and EDS analysis of the catalyst post reaction, which is summarized in Table 3. After 4 h of exposure to steam reforming conditions at 250 °C, the Zn was found to have replenished at the near surface region of the nanoparticles.

4. Conclusions

The inherent benefit for Pd/ZnO-based catalysts, over Cu/ZnO-based ones, is that the active site for the steam reforming of methanol is an alloyed Pd–Zn surface on the nanoparticle. After the catalyst has been deactivated over time, this alloy can be broken up by oxidation to PdO and ZnO, and the species are then reduced back to small nanoparticles with Pd–Zn surfaces under reaction conditions at 250 °C. Furthermore, it has been shown that different pretreatments can lead to changes in the surface Zn concentration and the extent of alloy formation. However, after reaction the Pd–Zn catalyst surfaces are seen be to restored, and based on the FTIR of adsorbed CO, appear to reach a similar state regardless of pretreatment. We hypothesize that the surface of the catalyst after each of the pretreatments is in a meta-stable state and it reorders and reaches equilibrium under reaction conditions. In other words, we have demonstrated that the $Pd/ZnO/Al_2O_3$ catalysts exhibit remarkable stability towards oxidation which is in contrast to conventional Cu/ZnO-based catalysts.

Acknowledgments

Financial support for this work was provided by the US Department of Energy, Grant DE-FG02-05ER15712. Additional support from the Power and Energy Consortium sponsored by the US Army Research Laboratory under the Collaborative Technology Alliance Program, Cooperative Agreement DAAD19-01-2-0010 and from NSF OISE 0730277 is also gratefully acknowledged. We would also like to thank BASF for supplying the commercial Cu/ZnO-based catalyst.

References

[1] D. Browning, P. Jones, K. Packer, J. Power Sources 65 (1997) 187.
[2] C.J. Jiang, D.L. Trimm, M.S. Wainwright, N.W. Cant, Appl. Catal. A 97 (1993) 145.
[3] N. Takezawa, N. Iwasa, Catal. Today 36 (1997) 45.
[4] N. Iwasa, S. Kudo, H. Takahashi, S. Masuda, N. Takezawa, Catal. Lett. 19 (1993) 211.
[5] N. Iwasa, S. Masuda, N. Ogawa, N. Takezawa, Appl. Catal. A 125 (1995) 145.
[6] N. Iwasa, S. Masuda, N. Takezawa, React. Kinet. Catal. Lett. 55 (1995) 349.
[7] N. Iwasa, T. Mayanagi, S. Masuda, N. Takezawa, React. Kinet. Catal. Lett. 69 (2000) 355.
[8] N. Iwasa, T. Mayanagi, W. Nomura, M. Arai, N. Takezawa, Appl. Catal. A 248 (2003) 153.
[9] N. Iwasa, T. Mayanagi, N. Ogawa, K. Sakata, N. Takezawa, Catal. Lett. 54 (1998) 119.
[10] N. Iwasa, N. Takezawa, Top. Catal. 22 (2003) 215.
[11] Z.X. Chen, K.M. Neyman, A.B. Gordienko, N. Rosch, Phys. Rev. B 68 (2003) 075417.
[12] K.H. Lim, L.V. Moskaleva, N. Rosch, ChemPhysChem. 7 (2006) 1802.
[13] K.M. Neyman, R. Sahnoun, C. Inntam, S. Hengrasmee, N. Rosch, J. Phys. Chem. B 108 (2004) 5424.
[14] J.A. Rodriguez, J. Phys. Chem. 98 (1994) 5758.
[15] A.P. Tsai, S. Kameoka, Y. Ishii, J. Phys. Soc. Jpn. 73 (2004) 3270.
[16] A. Karim, T. Conant, A. Datye, J. Catal. 243 (2006) 420.
[17] S. Penner, B. Jenewein, H. Gabasch, B. Klotzer, D. Wang, A. Knop-Gericke, R. Schlogl, K. Hayek, J. Catal. 241 (2006) 14.
[18] Z.X. Chen, K.M. Neyman, N. Rosch, Surface Sci. 548 (2004) 291.
[19] M. Baumer, J. Libuda, K.M. Neyman, N. Rosch, G. Rupprechter, H.J. Freund, Phys. Chem. Chem. Phys. 9 (2007) 3541.
[20] H. Borchert, B. Jurgens, V. Zielasek, G. Rupprechter, S. Giorgio, C.R. Henry, M. Baumer, J. Catal. 247 (2007) 145.
[21] M. Frank, M. Baumer, Phys. Chem. Chem. Phys. 2 (2000) 3723.
[22] C.R. Henry, Surf. Sci. Rep. 31 (1998) 235.
[23] E. Jeroro, V. Lebarbier, A. Datye, Y. Wang, J.M. Vohs, Surf. Sci. 601 (2007) 5546–5554.
[24] V. Lebarbier, R. Dagle, T. Conant, J.M. Vohs, A. Datye, Y. Wang, Catal. Lett. 122 (2008) 223.
[25] E.S. Ranganathan, S.K. Bej, L.T. Thompson, Appl. Catal. A 289 (2005) 153.
[26] N. Iwasa, W. Nomura, T. Mayanagi, S. Fujita, M. Arai, N. Takezawa, J. Chem. Eng. Jpn. 37 (2004) 286.
[27] H.S. Wu, S.C. Chung, J. Comb. Chem. 9 (2007) 990.